

Size and Shape Dependence of the Electronic Structure of Gold Nanoclusters on TiO₂

Chi-Ming Yim,^{†a} Philomena Schlexer Lamoureux,[‡] Andrew Mellor[†], Chi L. Pang,[†] Hicham Idriss[§], Gianfranco Pacchioni,[‡] and Geoff Thornton^{†*}

[†] Department of Chemistry and London Centre for Nanotechnology, University College London, 20 Gordon Street, London WC1H 0AJ, UK

[‡] Dipartimento di Scienza dei Materiali, Università degli Studi Milano-Bicocca, via R. Cozzi 55, 20126 Milano, Italy

[§] Surface Science and Advanced Characterisation, Chemical Sciences Division, SABIC-CRD at KAUST, Thuwal 23955, Saudi Arabia

AUTHOR INFORMATION

Corresponding Author

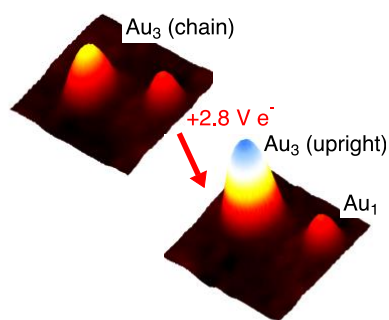
*To whom correspondence should be addressed. E-mail: g.thornton@ucl.ac.uk.

^a Current Address:

Tsung Dao Lee Institute and School of Physics and Astronomy, Shanghai Jiao Tong University, Shanghai 200240, China.

Abstract

Understanding the mechanism behind the superior catalytic power of single- or few-atom heterogeneous catalysts has become an important topic in surface chemistry. This is particularly the case for gold, with TiO_2 being an efficient support. Here we use scanning tunneling microscopy/spectroscopy with theoretical calculations to investigate the adsorption geometry and local electronic structure of several-atom Au clusters on rutile $\text{TiO}_2(110)$, with the clusters fabricated by controlled manipulation of single atoms. Our study confirms that Au_1 and Au_2 clusters prefer adsorption at surface O-vacancies. Au_3 clusters adsorb at O-vacancies in a linear-chain configuration parallel to the surface; in the absence of vacancies they adsorb at Ti_{5c} sites with a structure of a vertically pointing upright triangle. We find that both the electronic structure and cluster-substrate charge transfer depend critically on the cluster size, bonding configuration, and local environment. This suggests the possibility of engineering cluster selectivity for specific catalytic reactions.



KEYWORDS: gold, “several-atom” clusters, titanium dioxide, low electronic structure, scanning tunneling microscopy and spectroscopy

The catalytic properties of gold nanoparticles have received considerable attention since the discovery over three decades ago of low temperature CO oxidation catalysis by Au supported on metal oxides.¹ For many years it was thought that the optimum size of the nanoparticles is about 4 nm in diameter.² More recently, with the availability of aberration corrected transmission electron microscopy (TEM) results, it seems that much smaller particles could play an important role.³ A corollary is that the metal cluster/metal oxide interaction will be crucial to the catalytic activity.

More generally, “single atom” catalysts form a novel class of catalysts whose performance cannot be understood simply by using the conventional d-band model originally developed for extended metal surfaces.⁴ Instead, they are more akin to inorganic compounds involved in homogenous catalysis. Their unique properties, together with their superior catalytic performance,^{5,6} have sparked both theoretical and experimental interest from the surface science community,⁷ with the ultimate aim to unravel the underlying catalytic mechanisms.

Supported Au clusters exhibit unique catalytic properties.^{3,8} They also have application in areas such as photovoltaics⁹ and bio-sensing.¹⁰ As such, Au nanostructures, in particular those formed on metal oxide supports, have been widely investigated. Au nanoparticles supported on TiO₂ have long been a major study platform owing to their surprising catalytic behaviour^{1,2,11} and the fact that TiO₂(110) is a model oxide substrate.^{12–14} Recent work includes studies of reaction sites on nanostructure facets,^{15,16} the structure, size and shape of nanoparticles,^{2,17} as well as their charge state¹⁸ and their nucleation site.^{2,19} The charge state of Au atoms, clusters and nanoparticles has been a subject of considerable debate, with catalytic studies of CO oxidation concluding that cationic gold is the active catalyst. In contrast, surface science studies in ultrahigh vacuum (UHV) have found anionic gold to be present after the

growth of Au nanoparticles on TiO₂(110).^{17,19} This difference is thought to be due to the oxidizing conditions involved in the catalytic studies.²⁰

Scanning tunneling microscopy and spectroscopy (STM, STS) have been used in earlier work to obtain atomic scale information about the properties of supported nanostructures.^{21–23} Surface bridging O-vacancies V_O on reduced (*r*-) TiO₂(110) are found to be the most favoured adsorption site for both single Au atoms,^{21,24} which have an apparent height of ~1.9 Å in STM, and some small Au clusters.²⁵ Oxidizing the substrate to (*o*-) TiO₂(110) modifies the electronic structure of the clusters²⁶ as well as their adhesion strength.¹⁹ In part this can arise from the availability of adsorption sites, with V_O only being available on *r*-TiO₂(110). A difference in the electronic structure between Au₁ bound to V_O and to Ti_{5c} was recently observed, with metal induced gap states being observed for Ti_{5c}.²⁷ However, systematic studies of individual oxide-supported few-atom clusters with exact size and shape are lacking.²⁸

In this work we use a model system to explore the variation of Au cluster electronic structure with shape, size and adsorption site on an oxide substrate. TiO₂(110) is chosen as the model support. A combination of STM and density functional theory (DFT) is employed to probe clusters formed by controlled STM manipulation of single Au atoms. Our results determine unambiguously the bonding configuration and their associated electronic fingerprint for each cluster type with size up to nine atoms. The experimentally validated calculations predict that charge transfer between the Au clusters and the substrate depend strongly on the cluster size, bond geometry and local environment.

Figure 1a shows an STM topographic image of the reduced TiO₂(110) surface [*r*-TiO₂, characterized by surface O-vacancies (V_O)], taken after deposition of ~0.01 ML Au at room temperature. Additional features are formed on the surface after Au deposition: single Au adatoms residing at V_O [Au₁(V_O), marked by solid circles],²¹ and a number of small Au clusters, where Au₁ is found to be stable up to at least 600 K.²⁴

Previously we have demonstrated the use of voltage pulses in STM to study the bonding mechanism of single Au atoms on the TiO₂(110) surface.²¹ To establish a method to distinguish between different Au clusters, here we form Au clusters with exact sizes and shapes, achieved by displacing each of the Au adatoms using the voltage pulses. This is a similar approach is similar to that used to form small Pd clusters on MgO(001).²⁹ We note that Au atom transfer to the tip was not observed, as evidenced by the unchanged apex and the constant number of cluster gold atoms before and after each tip pulse. After forming the desired cluster we then study their electronic structure by tunneling spectroscopy in STM. Fig. 1, b and c demonstrate how voltage pulses (+3 V) were used to form an Au₂ species from two individual Au adatoms originally residing at V_{Os}. The Au₂ species formed is centered at V_O, which we therefore refer to as Au₂(V_O). An additional voltage pulse applied atop the Au₂(V_O) displaces it to the neighboring Ti_{5c} site, forming Au₂(Ti) (Fig. 1d).

To determine the bonding structure of the Au₂ clusters on the TiO₂(110) surface, we have performed DFT calculations. The calculations predict two low energy bonding configurations for Au₂(V_O) and Au₂(Ti) clusters, which are shown in Fig. 1, e and f, respectively. In the first configuration, Au atoms in the Au₂ cluster are bonded to each other as well as to the substrate Ti atoms beneath the O vacancy and bridging O atoms next to the vacancy ($r_{\text{Au-Au}} = 2.478 \text{ \AA}$). This configuration has a calculated adsorption energy (E_{ad}) of -1.86 eV. In the second configuration where no O vacancy is present on the surface (Fig. 1f), the Au atoms are aligned perpendicular to the O_b row direction and are bonded to each other, as well as to the in-plane Ti_{5c} atom, and the surrounding O atoms ($r_{\text{Au-Au}} = 2.523 \text{ \AA}$). This configuration has a slightly lower E_{ad} of -1.94 eV. Their simulated appearance in STM (Fig. 1, g and h), calculated using Tersoff-Hamann approach,³⁰ resemble those of the Au₂ clusters as observed in our experiment. The apparent size of Au₂(V_O) is smaller than Au₂(Ti), partly due to an effective difference in Au-Au distance, and partly to electronic effects.

Two types of Au₃ clusters were also formed on *r*-TiO₂(110). Fig. 2a shows an STM image of an Au₃ cluster formed by merging three single Au adatoms using +3 V tip pulses (see *Supporting Information* Fig. S1 for its step-by-step formation). The Au₃ cluster has a chain-like structure, with its left part, which resides above a V_O, appearing brighter than its right part in STM. This cluster has a measured height of ~2.85 Å (solid blue line plot in Fig. 2d). Comparing its height with that of a single atom verifies the flat morphology of the Au₃ cluster on the surface. Applying a +3 V tip pulse atop the cluster causes it to flip about the O_b row, so that it has the right side sitting above the V_O, and appearing brighter (Fig. 2b). This is corroborated by the line profiles taken across the cluster before and after flipping, which are mirror images of each other (Fig. 2d). We term this cluster type as Au₃(C), where C denotes a chain-like bonding configuration. We note that our finding also confirms the assignment of Au₃ clusters on *r*-TiO₂ in earlier work.¹⁹

Applying another +3 V pulse atop the Au₃(C) cluster in Fig. 2b leads to a significant change in its bonding configuration. Shown in Fig. 2c, the cluster now appears to have a round shape that is centered on a Ti_{5c} row. The cluster has a measured height of ~5.3 Å, indicative of an upright bonding configuration. On this basis, we term this newly formed cluster as Au₃(U), where U denotes the upright bonding configuration. In addition to voltage pulses, switching between the two configurations of Au₃ clusters can also result from an STM scan at an increased voltage (+2.4 V), see SI Fig. S2.

DFT calculations predict three possible bonding configurations for Au₃ on TiO₂(110) (Fig. 2, e to j). In one (Fig. 2, e and h), three Au atoms are bonded to each other in a chain. The Au atom on the left is at the V_O site, and is bonded to the Ti atoms beneath the vacancy. Gold atoms at the center and right of this asymmetric chain are bonded to a Ti_{5c} ion, and to the Ti_{5c} atom and in-plane O atoms, respectively ($r_{\text{Au-Au}} = 2.603$ Å and 2.519 Å, respectively). This bonding configuration has an E_{ad} of -3.14 eV. In the second configuration (Fig. 2, f and i),

three Au atoms are bonded to each other also in a chain-like fashion ($r_{\text{Au-Au}} = 2.528 \text{ \AA}$), but with the Au atoms on the sides bonded to the O_b ions. This configuration has a less favorable E_{ad} of -1.58 eV. In the third configuration (Figure 2, g and j), the Au atoms are bonded to each other in an upright triangular arrangement ($r_{\text{Au-Au}} = 2.573 \text{ \AA}$), with the Au atoms at the base also bonded to the O_b ions ($r_{\text{Au-Au}} = 2.918 \text{ \AA}$). This configuration has an E_{ad} of -2.88 eV, which is an adsorption energy approaching that of the asymmetric chain. The simulated appearance in STM of these three configurations is shown in Fig. 2, h-j. Their comparison with experiment indicates that the $\text{Au}_3(\text{C})$ cluster in Fig. 3a corresponds to the asymmetric chain-like bonding configuration shown in Fig. 2e, while $\text{Au}_3(\text{U})$ (Fig. 2c) corresponds to the upright bonding configuration in Fig. 2g. Note that in our experiment we have not observed an image of a Au_3 cluster that resembles that shown in Fig. 2i. SI Figs. S3, S4 show the step-by-step formation of larger Au clusters up to Au_9

Au clusters comprised of a few atoms are not strongly bound on $\text{TiO}_2(110)$.^{19,20} Therefore, they can be displaced or dispersed into smaller clusters by the STM tip even in moderate tunneling conditions. To minimize such tip-induced modifications during tunneling spectroscopy measurements, differential conductance (dI/dV) as a function of bias voltage (V) spectra were recorded in the closed feedback loop condition. In this scheme the tip-sample distance is varied in response to the voltage ramp so that the current (I) that flows across the tunneling junction is always maintained at its set-point value. This constant-current (cc-) tunneling spectroscopy mode has previously been used to study the molecular orbitals of single fullerene and their aggregates,²³ and for mapping the spatial variation of the surface work function within the MgO film on Mo(100).³¹ Further details about this spectroscopic method can be found in Refs ^{32,33}.

Fig. 3a presents a series of cc- dI/dV spectra recorded from the $\text{TiO}_2(110)$ substrate, as well as those from five different Au_n clusters, with their corresponding STM images shown in

Fig. 3, b to f. The spectra were recorded in the bias voltage range between 0.5 and 4 V above the Fermi level. We first discuss the spectra recorded from the TiO₂(110) substrate shown in Fig. 3a. The spectra obtained from the O_b (black) and Ti rows (grey) of the TiO₂(110) substrate exhibit two peaks each, one at ~2 V and another at 3 V. These two peaks correspond roughly to the t_{2g} and e_g antibonding orbitals of mainly Ti 3d character found in the bulk.^{34–36} However, their character will be modified by the surface sensitive nature of the measurement; for the DOS shown in Fig. 4a, 40% of the Ti atoms in the slab are five-fold coordinated.

The spectroscopic signatures of the Au_n clusters are markedly different both from each other and the substrate. The spectrum of the Au₁(V_O) cluster (red curve in Fig 3a) is characterized by two peaks: a shallow peak at 1.5 V and a very pronounced peak at 3.2 V. As for the Au₂ clusters, that of Au₂(V_O) (dark green) is characterized by two main peaks, one at 1.3 V and another at 2.4 V, and a shallow peak at 3.6 V. In the spectrum of Au₂(Ti) (light green), only two peaks are present, one at 1.7 V and another at 2.45 V. We attribute such shifts in the energy positions of the two major peaks in the spectra of the Au₂ clusters to the difference in the degrees of hybridization between the molecular orbitals of the Au₂ clusters and the substrate, arising from their different bonding geometries on the surface.³⁴

The spectra of the two types of Au₃ cluster are also very different. The spectrum of Au₃(C) (light blue) is characterized by two peaks, one at 1.45 V and another 2.2 V. On the other hand, that of Au₃(U) is characterized by a major peak at 2.4 V, and a very broad shoulder at ~0.7 V. This broad shoulder peak is also observed as a sharp peak at 1.2 V in the dI/dV spectrum of Au₃(U) recorded in the constant height condition (Fig. S5). Such energy shifts of peaks between the two spectroscopy modes have been explained systematically by the work of Hellenthal³² and Pronschinske et al.³³ Note that unlike the Au₁(V_O) and Au₂ clusters, the Au₃ clusters are rather unstable in spectroscopy measurements. They tend to hop, and switch

between the two bonding configurations at higher bias voltage (Fig. 3a). We have also recorded spectroscopy data from Au clusters of larger sizes, which are shown in Fig. S6.

DFT calculations are used to provide an understanding of the STS spectra and to examine cluster-substrate charge transfer. To elucidate the impact of V_O on the electronic structure of the adsorbed Au clusters, first we calculate the electronic structure of the $TiO_2(110)$ surface in both the stoichiometric (s - TiO_2) and in the reduced form (r - TiO_2). Here s - TiO_2 was modeled in the slab calculations by having five TiO_2 layers with 3×2 TiO_2 unit cells per layer with each slab, and separation distance of $>12 \text{ \AA}$ between slabs. r - TiO_2 was modeled by removing an O_b at the surface, leaving two excess electrons in the TiO_2 slabs as a result of the V_O formation. This results in surface O vacancy concentration of 16.7% in the model (see SI Computational Details). It is well established that when it comes to calculating the electronic structure of the $TiO_2(110)$ surface, DFT with the generalized gradient approximation (GGA) approach suffers from the so-called self-interaction error, leading to the erroneous descriptions of the (i) TiO_2 band-gap, (ii) the Ti 3d defect state within the band gap (namely band gap state, or BGS), and (iii) the localization of the excess electrons. To partly correct this error, we have used the DFT+U approach, with the Hubbard U parameter set at 3 eV for the Ti 3d states (see SI Computational Details). With this scheme we find a band-gap of 1.92 eV for s - TiO_2 (Fig. 4a), which is still ~ 1 eV less than the experimentally found bulk value of ~ 3 eV.³⁵ On r - TiO_2 , we find that the BGS lies ~ 0.6 eV below the conduction band minimum (CBM). This is in reasonable agreement with photoemission data, where the BGS lies ~ 0.8 eV below E_F .³⁶ The V_O -associated excess electrons are localized at two different sub-surface Ti ions, resulting in a triplet state (Fig. 4c). This is in good agreement with the work of Morgan *et al.*³⁷

The calculated projected density of states (PDOS) of the Au clusters are shown in Fig. 4, d-i. Depending on their bonding configurations, the PDOS were calculated with either s - or r - TiO_2 as the substrate. We first discuss the results for $Au_1(V_O)$, calculated on r - TiO_2 . As

shown in Fig. 4d, the Au 6s state at around 1 eV below CBM is completely filled, indicating that one of the excess electrons is transferred from the substrate to the Au atom. Such charge transfer leads to a negatively charged Au₁ species (Bader charge -0.48 |e|, Table 1), with a significantly increased adsorption energy of 1.7 eV³⁸-1.81 eV.³⁴

A number of unfilled states are also present above the CBM. As for the results of Au₂(Ti) calculated on *s*-TiO₂ (Fig. 4e), its PDOS has a closed-shell Au 6s states just above the valence band maximum (VBM) of the substrate, which we assign to the Au-Au bond formation; a corresponding antibonding component with 6s character can be observed at about 2 eV above the CBM. No major charge transfer between Au₂(Ti) and *s*-TiO₂ occurs, as confirmed also by the Bader charges on Au seen in Table 1. This also holds true for Au₂(V_O). Shown in Fig. 4f, the filled Au 6s states of Au₂(V_O) shift slightly towards lower energies going from the *s*- to *r*-TiO₂ supports. This could be due to the stabilization of those states by interaction of the highest occupied molecular orbital (HOMO) of the Au₂ species with the excess electrons at V_O sites, or increased overlap of its HOMO with the surface states of the *r*-TiO₂ localized on the bridging and the in-plane oxygen atoms, or a combination of both.³⁴ A very pronounced 6s antibonding state can be observed at about 2 eV above the CBM, Fig. 4(f).

The Au₃ clusters exhibit a doublet state in the gas-phase. As noted above, Au₃ adopts one of the two bonding configurations on *s*-TiO₂, namely the flat, symmetric chain-like configuration [Au₃(C)], and the upright triangle configuration [Au₃(U)]. Both of these configurations lead to singlet states (Fig. 4, g and h). For Au₃(C) on *s*-TiO₂, pronounced unfilled Au states with 6s character are observed just at the CBM (Fig. 4g), and are shifted to ~0.5 eV above the CBM for Au₃(U) (Fig. 4h). For both Au₃ clusters on *s*-TiO₂, an occupied Ti 3d state within the TiO₂ band gap is found, hinting that electron transfer is from the Au₃ clusters to the substrate. This is corroborated by a Bader charge of +0.13 |e| per Au atom seen in Table 1. Compared to Au₃(C), the Au₃(U) on *s*-TiO₂ has a significantly higher energy

splitting of its HOMO and lowest unoccupied molecular orbital (LUMO). This accounts for the much greater calculated stability of the Au₃(U) cluster on *s*-TiO₂ (Fig. 2) compared with the symmetric chain. The amount of charge transfer from Au₃(U) to TiO₂, however, is similar (see Table 1).

Fig. 4i shows the PDOS calculated for a Au₃ cluster adsorbed on *r*-TiO₂ in a chain-like structure. This corresponds to the Au₃(C) cluster shown in the STM image in Fig. 2a. This cluster has its HOMO to LUMO splitting approximately the same as that of Au₃(U) on *s*-TiO₂, meaning that the Au₃(C) is stable on the reduced surface when formed. Intriguingly, its formation on *r*-TiO₂ results in a BGS which is noticeably smaller than that for Au₂(V_O). This suggests electron transfer from the oxide support to the Au₃ cluster. This is consistent with the presence of two 6s-derived Au₃ orbitals below the Fermi level, pointing to the formation of a Au₃⁻ species. Indeed, the Bader analysis shows that now the Au atoms have an average charge of -0.16 |e| each. Results of the calculated charge transfer directions for different clusters as well as their adsorption energies are summarized in Table 1. The electronic structure of Au trimers is relatively simple, with the Au atom 5d shell being filled. They do not contribute substantially to the bonding, which is dominated by 6s interactions that give rise to bonding, non-bonding, and anti-bonding states. On the stoichiometric support only the bonding 6s state is filled, and Au₃ carries a positive charge; on the reduced support, also the non-bonding state is filled, and Au₃ carries a negative charge. The energy minimized structures of the clusters calculated in this work differ to an extent from those calculated in earlier work³⁴, which can be ascribed to the different computational methodology employed (PBE+U with dispersion present work, PW91 in ref³⁴). Nevertheless, there is good qualitative agreement in the cluster adsorption energies and charge transfer directions.

The Au clusters formed on the TiO₂(110) surface are characterized by a number of occupied and unoccupied Au states in the electronic structure (Fig. 4). The combination of

these states is unique for each Au cluster type. For example, open shell species such as Au₁ or Au₃ tend to exchange electrons with the support (Au₃ behaves as an electron donor on *s*-TiO₂ and Au₁ and Au₃ act as electron acceptors on *r*-TiO₂), while closed shell species such as Au₂ are covalently bound to the support. This suggests the possibility of identifying the size and geometry of a cluster by comparing STS data with the results of DFT calculations. To validate this idea on a qualitative basis, we compare the energy positions observed in tunneling spectroscopy for each cluster type with those predicted by the Au DOS obtained from DFT (see Fig. S7). Good agreement is observed apart from the Au₁ results, where the experimental spectra are expected to be strongly influenced by the substrate.

In summary, we have used STM tip pulsing of Au atoms at oxygen vacancies on TiO₂(110) to create Au₂ and Au₃ clusters with varying geometries and adsorption sites. Using STS and STM topographic data in combination with DFT calculations, we find that the electronic structure of the clusters is critically dependent on both the shape and anchoring site of the clusters. This includes the direction of charge transfer to the substrate, with both anionic and cationic gold clusters being formed. Our study therefore provides insights for the design of few-atom Au catalysts on TiO₂ supports for optimal catalytic performance. Moreover, the rapid change in properties with the number of Au atoms in a cluster is in line with the prediction of a hierarchy of activity with the size of supported Au clusters.³

ASSOCIATED CONTENT

Supporting Information. The following files are available free of charge.

Experimental Details, Computational Details, Supporting Figs. S1-S6.

AUTHOR INFORMATION

Notes

The authors declare no competing financial interests.

ACKNOWLEDGMENTS

G.P. and P.S.L. thank Dr. Farahnaz Maleki for useful discussions. This work was supported by the European Research Council Advanced Grant ENERGYSURF, EPSRC (UK)-EP/G036675/1, the Royal Society through a Wolfson Merit Award to GT, and the Alexander von Humboldt Stiftung. Financial support from the Italian Ministry of University and Research (MIUR) through PRIN Project 20179337R7 MULTI-e “Multielectron transfer for the conversion of small molecules: an enabling technology for the chemical use of renewable energy”, and the grant Dipartimenti di Eccellenza - 2017 "Materials For Energy" is gratefully acknowledged.

REFERENCES

- (1) Haruta, M. Size- and Support-Dependency in the Catalysis of Gold. *Catal. Today* **1997**, *36* (1), 153–166. [https://doi.org/10.1016/S0920-5861\(96\)00208-8](https://doi.org/10.1016/S0920-5861(96)00208-8).
- (2) Chen, M. S.; Goodman, D. W. The Structure of Catalytically Active Gold on Titania. *Science* **2004**, *306*, 5.
- (3) Hutchings, G. J. Heterogeneous Gold Catalysis. *ACS Cent. Sci.* **2018**, *4* (9), 1095–1101. <https://doi.org/10.1021/acscentsci.8b00306>.
- (4) Hammer, B.; Morikawa, Y.; Nørskov, J. K. CO Chemisorption at Metal Surfaces and Overlayers. *Phys. Rev. Lett.* **1996**, *76* (12), 2141–2144. <https://doi.org/10.1103/PhysRevLett.76.2141>.
- (5) Qiao, B.; Wang, A.; Yang, X.; Allard, L. F.; Jiang, Z.; Cui, Y.; Liu, J.; Li, J.; Zhang, T. Single-Atom Catalysis of CO Oxidation Using Pt₁/FeO_x. *Nature Chem* **2011**, *3* (8), 634–641. <https://doi.org/10.1038/nchem.1095>.
- (6) Cheng, N.; Zhang, L.; Doyle-Davis, K.; Sun, X. Single-Atom Catalysts: From Design to Application. *Electrochem. Energ. Rev.* **2019**, *2* (4), 539–573. <https://doi.org/10.1007/s41918-019-00050-6>.
- (7) Hulva, J.; Meier, M.; Bliem, R.; Jakub, Z.; Kraushofer, F.; Schmid, M.; Diebold, U.; Franchini, C.; Parkinson, G. S. Unraveling CO Adsorption on Model Single-Atom Catalysts. *Science* **2021**, *371* (6527), 375–379. <https://doi.org/10.1126/science.abe5757>.
- (8) Thompson, D. T. Using Gold Nanoparticles for Catalysis. *Nano Today* **2007**, *2* (4), 40–43. [https://doi.org/10.1016/S1748-0132\(07\)70116-0](https://doi.org/10.1016/S1748-0132(07)70116-0).
- (9) Giangregorio, M. M.; Losurdo, M.; Bianco, G. V.; Dilonardo, E.; Capezzuto, P.; Bruno, G. Synthesis and Characterization of Plasmon Resonant Gold Nanoparticles and Graphene for Photovoltaics. *Mater. Sci. Eng.: B* **2013**, *178* (9), 559–567. <https://doi.org/10.1016/j.mseb.2012.10.034>.
- (10) Zeng, S.; Yong, K.-T.; Roy, I.; Dinh, X.-Q.; Yu, X.; Luan, F. A Review on Functionalized Gold Nanoparticles for Biosensing Applications. *Plasmonics* **2011**, *6* (3), 491–506. <https://doi.org/10.1007/s11468-011-9228-1>.
- (11) Herzing, A. A.; Kiely, C. J.; Carley, A. F.; Landon, P.; Hutchings, G. J. Identification of Active Gold Nanoclusters on Iron Oxide Supports for CO Oxidation. *Science* **2008**, *321* (5894), 1331–1335. <https://doi.org/10.1126/science.1159639>.
- (12) Diebold, U. The Surface Science of Titanium Dioxide. *Surf. Sci. Rep.* **2003**, *48* (5–8), 53–229. [https://doi.org/10.1016/S0167-5729\(02\)00100-0](https://doi.org/10.1016/S0167-5729(02)00100-0).
- (13) Pang, C. L.; Lindsay, R.; Thornton, G. Chemical Reactions on Rutile TiO₂(110). *Chem. Soc. Rev.* **2008**, *37* (10), 2328. <https://doi.org/10.1039/b719085a>.
- (14) Henderson, M. A. A Surface Science Perspective on TiO₂ Photocatalysis. *Surf. Sci. Rep.* **2011**, *66* (6–7), 185–297. <https://doi.org/10.1016/j.surfrep.2011.01.001>.
- (15) Boyle, D. T.; Wilke, J. A.; Palomino, R. M.; Lam, V. H.; Schlosser, D. A.; Andahazy, W. J.; Stopak, C. Z.; Stacchiola, D. J.; Rodriguez, J. A.; Baber, A. E. Elucidation of Active Sites for the Reaction of Ethanol on TiO₂/Au(111). *J. Phys. Chem. C* **2017**, *121* (14), 7794–7802. <https://doi.org/10.1021/acs.jpcc.6b11764>.
- (16) Green, I. X.; Tang, W.; Neurock, M.; Yates, J. T. Insights into Catalytic Oxidation at the Au/TiO₂ Dual Perimeter Sites. *Acc. Chem. Res.* **2014**, *47* (3), 805–815. <https://doi.org/10.1021/ar400196f>.
- (17) Mellor, A.; Wilson, A.; Pang, C. L.; Yim, C. M.; Maccherozzi, F.; Dhesi, S. S.; Muryn, C. A.; Idriss, H.; Thornton, G. Photoemission Core Level Binding Energies from Multiple Sized Nanoparticles on the Same Support: TiO₂(110)/Au. *J. Chem. Phys.* **2020**, *152* (2), 024709. <https://doi.org/10.1063/1.5135760>.

- (18) Wei, S.; Fu, X.-P.; Wang, W.-W.; Jin, Z.; Song, Q.-S.; Jia, C.-J. Au/TiO₂ Catalysts for CO Oxidation: Effect of Gold State to Reactivity. *J. Phys. Chem. C* **2018**, *122* (9), 4928–4936. <https://doi.org/10.1021/acs.jpcc.7b12418>.
- (19) Matthey, D.; Wang, J. G.; Wendt, S.; Matthiesen, J.; Schaub, R.; Lægsgaard, E.; Hammer, B.; Besenbacher, F. Enhanced Bonding of Gold Nanoparticles on Oxidized TiO₂(110). *Science* **2007**, *315* (5819), 1692–1696. <https://doi.org/10.1126/science.1135752>.
- (20) Panayotov, D. A.; Morris, J. R. Surface Chemistry of Au/TiO₂: Thermally and Photolytically Activated Reactions. *Surf. Sci. Rep.* **2016**, *71* (1), 77–271. <https://doi.org/10.1016/j.surfrep.2016.01.002>.
- (21) Mellor, A.; Humphrey, D.; Yim, C. M.; Pang, C. L.; Idriss, H.; Thornton, G. Direct Visualization of Au Atoms Bound to TiO₂ (110) O-Vacancies. *J. Phys. Chem. C* **2017**, *121* (44), 24721–24725. <https://doi.org/10.1021/acs.jpcc.7b09608>.
- (22) Yim, C. M.; Pang, C. L.; Hermoso, D. R.; Dover, C. M.; Murn, C. A.; Maccherozzi, F.; Dhesi, S. S.; Pérez, R.; Thornton, G. Influence of Support Morphology on the Bonding of Molecules to Nanoparticles. *Proc Natl Acad Sci USA* **2015**, *112* (26), 7903–7908. <https://doi.org/10.1073/pnas.1506939112>.
- (23) Feng, M.; Zhao, J.; Petek, H. Atomlike, Hollow-Core-Bound Molecular Orbitals of C₆₀. *Science* **2008**, *320* (5874), 359–362. <https://doi.org/10.1126/science.1155866>.
- (24) Tong, X.; Benz, L.; Chrétien, S.; Metiu, H.; Bowers, M. T.; Buratto, S. K. Direct Visualization of Water-Induced Relocation of Au Atoms from Oxygen Vacancies on a TiO₂(110) Surface. *J. Phys. Chem. C* **2010**, *114* (9), 3987–3990. <https://doi.org/10.1021/jp9098705>.
- (25) Wahlström, E.; Lopez, N.; Schaub, R.; Thostrup, P.; Rønnau, A.; Africh, C.; Lægsgaard, E.; Nørskov, J. K.; Besenbacher, F. Bonding of Gold Nanoclusters to Oxygen Vacancies on Rutile TiO₂(110). *Phys. Rev. Lett.* **2003**, *90* (2), 026101. <https://doi.org/10.1103/PhysRevLett.90.026101>.
- (26) Adachi, Y.; Wen, H. F.; Zhang, Q.; Miyazaki, M.; Sugawara, Y.; Li, Y. J. Elucidating the Charge State of an Au Nanocluster on the Oxidized/Reduced Rutile TiO₂(110) Surface Using Non-Contact Atomic Force Microscopy and Kelvin Probe Force Microscopy. *Nanoscale Adv.* **2020**, *2* (6), 2371–2375. <https://doi.org/10.1039/C9NA00776H>.
- (27) Dong, S.; Li, B.; Cui, X.; Tan, S.; Wang, B. Photoresponses of Supported Au Single Atoms on TiO₂(110) through the Metal-Induced Gap States. *J. Phys. Chem. Lett.* **2019**, *10* (16), 4683–4691. <https://doi.org/10.1021/acs.jpcclett.9b01527>.
- (28) Nilus, N.; Ganduglia-Pirovano, M. V.; Brázdová, V.; Kulawik, M.; Sauer, J.; Freund, H.-J. Electronic Properties and Charge State of Gold Monomers and Chains Adsorbed on Alumina Thin Films on NiAl(110). *Phys. Rev. B* **2010**, *81* (4), 045422. <https://doi.org/10.1103/PhysRevB.81.045422>.
- (29) Sterrer, M.; Risse, T.; Giordano, L.; Heyde, M.; Nilus, N.; Rust, H.-P.; Pacchioni, G.; Freund, H.-J. Palladium Monomers, Dimers, and Trimers on the MgO(001) Surface Viewed Individually. *Angew. Chem. Int. Edit.* **2007**, *46* (45), 8703–8706. <https://doi.org/10.1002/anie.200702444>.
- (30) Tersoff, J.; Hamann, D. R. Theory of the Scanning Tunneling Microscope. *Phys. Rev. B* **1985**, *31* (2), 805–813. <https://doi.org/10.1103/PhysRevB.31.805>.
- (31) Pauly, C.; Grob, M.; Pezzotta, M.; Pratzner, M.; Morgenstern, M. Gundlach Oscillations and Coulomb Blockade of Co Nanoislands on MgO/Mo(100) Investigated by Scanning Tunneling Spectroscopy at 300 K. *Phys. Rev. B* **2010**, *81* (12), 125446. <https://doi.org/10.1103/PhysRevB.81.125446>.

- (32) Hellenthal, C.; Heimbuch, R.; Sotthewes, K.; Kooij, E. S.; Zandvliet, H. J. W. Determining the Local Density of States in the Constant Current STM Mode. *Phys. Rev. B* **2013**, *88* (3), 035425. <https://doi.org/10.1103/PhysRevB.88.035425>.
- (33) Pronschinske, A.; Mardit, D. J.; Dougherty, D. B. Modeling the Constant-Current Distance-Voltage Mode of Scanning Tunneling Spectroscopy. *Phys. Rev. B* **2011**, *84* (20), 205427. <https://doi.org/10.1103/PhysRevB.84.205427>.
- (34) Chrétien, S.; Metiu, H. Density Functional Study of the Interaction between Small Au Clusters, Aun (N=1–7) and the Rutile TiO₂ Surface. II. Adsorption on a Partially Reduced Surface. *The Journal of Chemical Physics* **2007**, *127* (24), 244708. <https://doi.org/10.1063/1.2806802>.
- (35) Rocker, G.; Schaefer, J. A.; Göpel, W. Localized and Delocalized Vibrations on TiO₂(110) Studied by High-Resolution Electron-Energy-Loss Spectroscopy. *Phys. Rev. B* **1984**, *30* (7), 3704–3708. <https://doi.org/10.1103/PhysRevB.30.3704>.
- (36) Yim, C. M.; Pang, C. L.; Thornton, G. Oxygen Vacancy Origin of the Surface Band-Gap State of TiO₂(110). *Phys. Rev. Lett.* **2010**, *104* (3), 036806. <https://doi.org/10.1103/PhysRevLett.104.036806>.
- (37) Morgan, B. J.; Watson, G. W. A DFT+U Description of Oxygen Vacancies at the TiO₂ Rutile (110) Surface. *Surf. Sci.* **2007**, *601* (21), 5034–5041. <https://doi.org/10.1016/j.susc.2007.08.025>.
- (38) Wörz, A. S.; Heiz, U.; Cinquini, F.; Pacchioni, G. Charging of Au Atoms on TiO₂ Thin Films from CO Vibrational Spectroscopy and DFT Calculations. *J. Phys. Chem. B* **2005**, *109* (39), 18418–18426. <https://doi.org/10.1021/jp054093o>.

Table 1. A table listing for each of Au cluster type the substrate used (reduced or stoichiometric TiO₂) in the calculations, the calculated adsorption energies, and the direction and magnitude of electron transfer between the Au cluster and the TiO₂ substrate for each Au cluster type

	Substrate type	Calculated E _{ad} (eV)	Direction of electron transfer Au _n ↔ TiO ₂	Computed Bader charge on Au atoms	Au cluster experimentally observed?
Au ₁ (Vo)	Reduced	--	←	-0.48	Yes
Au ₂ (Vo)	Reduced	-1.93	No	0.00	Yes
Au ₂ (Ti)	Stoichiometric	-1.86	No	+0.03	Yes
Au ₃ (C)	Reduced	-2.88	←	-0.16	Yes
	Stoichiometric	-1.58	→	+0.13	No
Au ₃ (U)	Stoichiometric	-3.14	→	+0.15	Yes

FIGURES

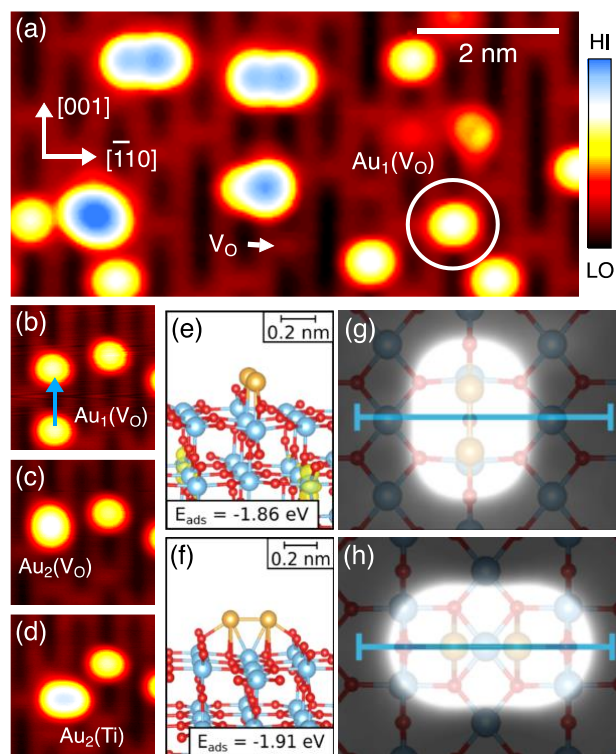


Figure 1. (a) STM image of r-TiO₂ recorded at 78 K after deposition of ~0.01 ML Au at room temperature. A circle marks single Au adatoms at V_O sites [Au₁(V_O)]. (b-c) Images taken (b) before and (c) after the formation a Au₂ cluster centered at V_O [Au₂(V_O)], by combining two individual Au adatoms using +3 V tip pulses. (d) Image of a Au₂ cluster centered at Ti_{5c} site [Au₂(Ti)], formed as a result of a tip pulse applied atop the Au₂(V_O) in (c). Image size: (a) 8×4 nm², (b-d) 3×3 nm². Scanning parameters: (a) 0.8 V, 0.1 nA, (b) 1 V, 0.1 nA, (c) 1 V, 20 pA, (d) 0.8 V, 15 pA. (e-f) Ball and stick models of the calculated minimum energy structures of Au₂(V_O) (e) and Au₂(Ti) (f) clusters on the TiO₂(110) surface. (g-h) Corresponding simulated STM images, calculated with sample bias set at 0.8 V, d(Au-tip) = 1.00 Å, and iso-surface of 1×10⁻⁷ |e|/Å³. In (g-h), scale bars indicate a span of 1 nm along the $[\bar{1}10]$ direction.

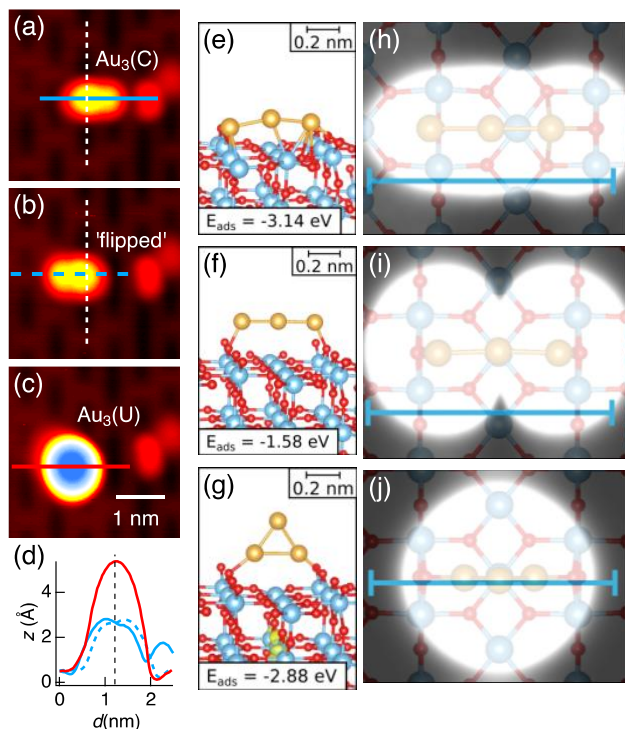


Figure 2. (a) STM image of a $\text{Au}_3(\text{C})$ cluster. (b) As (a), taken after the $\text{Au}_3(\text{C})$ cluster in (a) was flipped about the O_b row by a +3 V tip pulse. (c) As (b), taken after the $\text{Au}_3(\text{C})$ cluster in (b) was transformed to an upright bonding configuration by another tip pulse, becoming a $\text{Au}_3(\text{U})$ cluster. Image size: $(3.5 \text{ nm})^2$. Scan parameters: 0.8 V, 0.1 nA. (d) Line profiles measured across the $\text{Au}_3(\text{C})$ clusters in (a-b) (solid and dashed blue), and the $\text{Au}_3(\text{U})$ in (c) (red). (e-g) Side-view ball and stick models of the calculated structures for Au_3 cluster in three different bonding configurations on the $\text{TiO}_2(110)$ surface: (e-f) the chain-like configurations (e) with and (f) without the presence of surface V_O , and (g) upright configuration. In the models, red, blue and orange spheres represent O, Ti and Au atoms, respectively. (h-j) The corresponding top-view models overlaid with the simulated STM images calculated for each Au_3 structure in (e-g). The simulated images were calculated with sample bias set at 0.8 V, $d(\text{Au-tip}) = 1.00 \text{ \AA}$, and an iso-surface of $1 \times 10^{-6} |e|/\text{\AA}^3$. Scale bar = 1 nm.

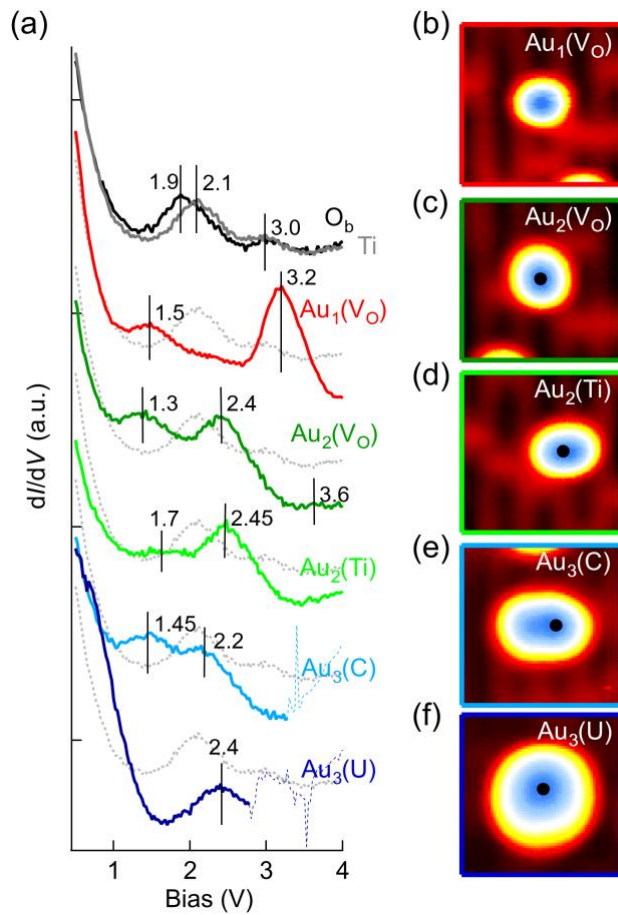


Figure 3. (a) Constant-current (cc-) dI/dV spectra recorded from the $\text{TiO}_2(110)$ substrate (black: O_b , grey: Ti_{5c}), as well as from different Au_n clusters shown in the topographic images in (b-f). Spectra obtained from the Ti_{5c} row are overlaid on top of those of the Au_n clusters for visual guidance. Spectra are vertically offset for clarity. Spectroscopy set-point = 20 pA. (b-f) Atomically resolved images of different Au cluster types, including (b) $\text{Au}_1(\text{V}_\text{O})$, (c) $\text{Au}_2(\text{V}_\text{O})$, (d) $\text{Au}_2(\text{Ti})$, (e) $\text{Au}_3(\text{C})$, and (f) $\text{Au}_3(\text{U})$. Image size $(2.4 \text{ nm})^2$. Scanning parameters (V, I): (b-d) 1.4 V, 0.1 nA, (e) 1 V, 0.1 nA, (f) 1.5 V, 50 pA. In each image, the black dot indicates the position at which the corresponding spectrum in (a) was recorded.

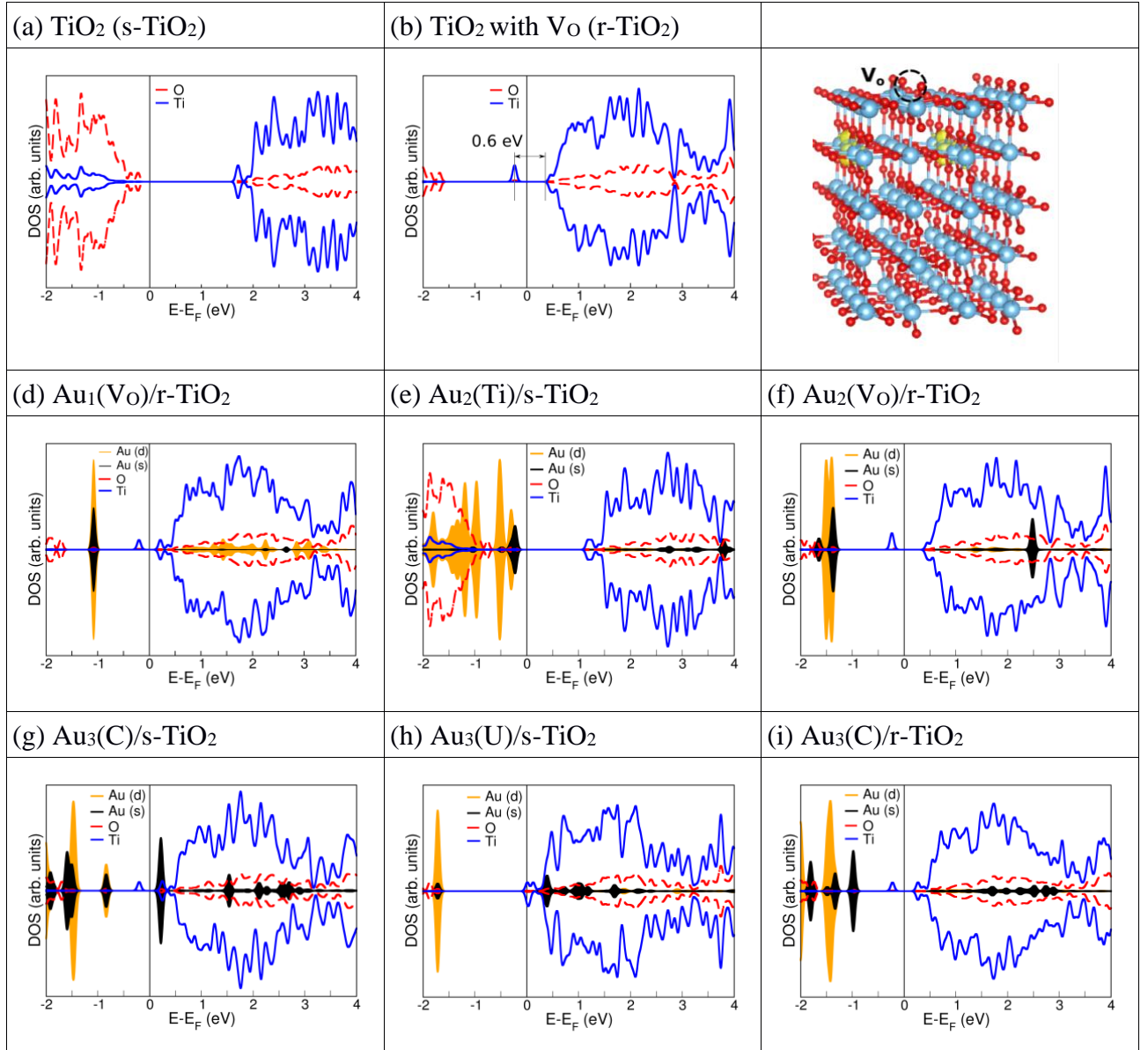


Figure 4. (a-b) Calculated projected density of states (PDOS) of the (a) stoichiometric (s-TiO₂) and (b) reduced surfaces (r-TiO₂) of rutile TiO₂(110), the latter of which contains one surface V_O and two excess electrons in the TiO₂ slabs. In (b), Ti 3d BGS are located 0.6 eV below the CBM. (c) Spin-density iso-surface, 0.01 |e|/Å³, of r-TiO₂. (d-h) Calculated PDOS of different Au clusters on the TiO₂(110) surface. The PDOS of the (d) Au₁(V_O), (f) Au₂(V_O), and (i) Au₃(C) were calculated on the r-TiO₂, while those of the (e) Au₂(Ti), (h) Au₃(U) and (i) another type of Au₃(C) were calculated using s-TiO₂ as the substrate. In (d-i), the energy of the CBM is set to zero to facilitate direct comparison between the PDOS and STS data.